ACS APPLIED MATERIALS & INTERFACES

Research Article

Synthesis and in Vitro Evaluation of Bone-Seeking Superparamagnetic Iron Oxide Nanoparticles as Contrast Agents for Imaging Bone Metabolic Activity

Arash Panahifar,[†] Morteza Mahmoudi,[‡] and Michael R. Doschak*[,†,§]

[†]Faculty of Pharmacy & Pharmaceutical Sciences and [§]Department of Biomedical Engineering, Faculty of Medicine, University of Alberta, Edmonton, Alberta, Canada

[‡]Department of Nanotechnology, Faculty of Pharmacy, Tehran University of Medical Sciences, Tehran, Iran

ABSTRACT: In this article, we report the synthesis and in vitro evaluation of a new class of nonionizing bone-targeting contrast agents based on bisphosphonate-conjugated superparamagnetic iron oxide nanoparticles (SPIONs), for use in imaging of bone turnover with magnetic resonance imaging (MRI). Similar to bone-targeting ^{99m}Technetium medronate, our novel contrast agent uses bisphosphonates to impart bone-seeking properties, but replaces the former radioisotope with nonionizing SPIONs which enables their subsequent detection using MRI. Our reported method is relatively simple, quick and cost-effective and results in BP-SPIONs with a final nanoparticle size of 17 nm under electron microscopy technique (i.e., TEM). In-vitro binding studies of our novel bone tracer have shown selective binding affinity (around 65%) for hydroxyapatite, the principal mineral of bone. Bone-targeting SPIONs offer the potential for use as nonionizing MRI contrast agents capable of imaging dynamic bone turnover, for use in the diagnosis and monitoring of metabolic bone diseases and related bone pathology.

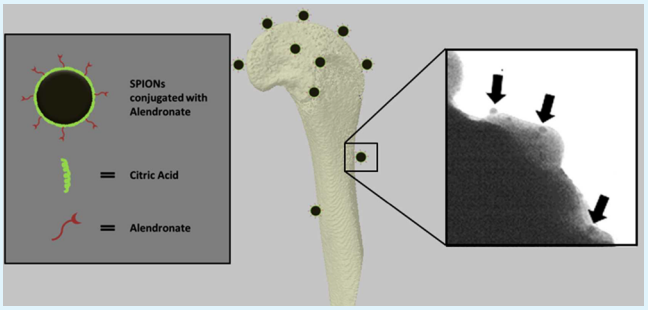

KEYWORDS: *bisphosphonate, superparamagnetic iron oxide nanoparticles, diagnosis, MRI, contrast agent, selective binding, bone, osteoarthritis*

1. INTRODUCTION

Bone disorders such as osteoarthritis (OA) and osteoporosis are responsible for high percentage of economic burden globally. OA alone affects approximately 27 million adults in United States.[1] It is a chronic condition and is usually diagnosed in advanced stages, where treatment options are limited to pain management or surgical joint replacement. Accordingly, the early diagnosis of OA and other metabolic conditions of aberrant bone turnover plays a vital role in treatment and disease management. The current gold standard for diagnosis of OA is X-ray radiography to measure joint space narrowing, as an indirect measure of cartilage loss. However, it is important to recognize that OA can be further characterized by temporal sequelae of periarticlular bone remodeling activity during disease pathogenesis, in a compartmental and site-specific manner.[2,3] Although a topic of controversy, it has been suggested that adaptations in bone potentially precede subsequent cartilage degradation.[4] Nuclear medicine is capable of imaging dynamic bone turnover by bone scintigraphy, which involves the intravenous administration of bisphosphonate based bone-targeting radioactive tracers, notably ^{99m}Tc-MDP (Methylene Diphosphonate). Dieppe et al.[5] showed that bone scintigraphy can predict cartilage loss prior to the appearance of radiographic changes. We recently reported the same using stable and nonionizing elemental strontium (as a surrogate for calcium) to map the metabolic activity of bone in osteoarthritic rats, and detected the formation of osteophytes prior to their radiological appearance under micro-computed tomography.[6]

On the other hand, magnetic resonance imaging (MRI) is a powerful diagnostic modality for the noninvasive imaging of cartilage, as well as inflammation related features such as synovitis and bone marrow lesion. MRI is generally limited to structural information, however, it can also detect dynamic physiological activity when functional contrast agents uptaken by a particular metabolic process are employed.[7] Currently ,there is no MRI contrast agent for imaging bone turnover. Contrast agents capable of targeting bone would offer the possibility for imaging bone metabolic activity under MRI, while additionally providing common structural findings at the same time, simply by changing the MRI sequence. Superparamagnetic iron oxide nanoparticles (SPIONs) are recognized as one of the most promising candidates for biomedical applications because their biocompatibility and unique magnetic properties.[8] Recently, the use of bisphosphonates

Received: March 22, 2013
Accepted: May 14, 2013
Published: May 14, 2013

   dx.doi.org/10.1021/am4010495 | *ACS Appl. Mater. Interfaces* 2013, 5, 5219−5226

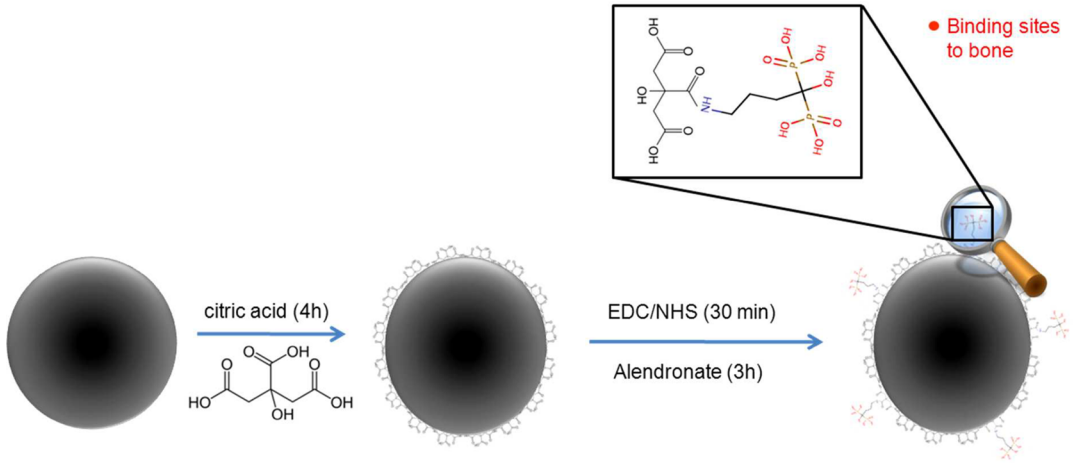

Figure 1. Schematic picture indicating the preservation of ALN phosphonate moieties during conjugation to SPIONs, for subsequent targeting of bone.

(BP) anchored to SPIONs has attracted attention.[9,10] BPs are the first-line treatment option for treatment of metabolic bone diseases characterized by excessive bone resorption such as osteoporosis or Paget's disease. They inhibit osteoclast-mediated bone resorption, thus returning bone metabolism to homeostasis. The mechanism by which BPs target the remodeling bone is attributed to their molecular P−C−P structural backbone, wherein they serve as analogue of inorganic pyrophosphate and adsorb onto calcium-phosphate (hydroxyapatite) matrix of bone. Phosphonate groups are the main binding groups of BPs with some contribution in the case of R_1 OH group, or nitrogen in nitrogen-containing BPs that can form hydrogen bond with hydroxyapatite (HA) crystal. Depending on R_1, they can attach to the calcium surface in bidentate (i.e., PO_3) or tridentate (i.e., PO_3 and OH).[11] However, phosphonate functional groups are also known to complex strongly with iron molecular structures.[12] Therefore, to achieve the successful targeting of bone, it is crucial to prevent the phosphonate functional groups of BPs from binding directly to the surface of SPIONs. Thus, in the present work, we have taken extensive effort to preserve the active phosphonate functional groups for subsequent targeting of bone. The nitrogen-containing BP, alendronate (ALN), was used as the bone targeting moiety and conjugated to SPIONs as the MRI visible moiety. Bone targeting potential of the compound was characterized in vitro using hydroxyapatite

2. EXPERIMENTAL METHODS

2.1. Materials. $FeCl_2$·tetra-hydrate (≥99%), $FeCl_3$·hexa-hydrate (≥99%), 1-butanol (≥99%), EDC (N-ethyl-N′-[3(dimethylamino)-propyl]carbodiimide hydrochloride), citric acid (≥99%), and nitric acid (70%) were purchased from Sigma-Aldrich (USA). Alendronate sodium trihydrate (≥97%) and CTAB (hexadecyltrimethylammonium bromide, ≥99%) were purchased from Sigma (USA). NHS (N-hydroxysuccinimide, ≥98%) was from Aldrich (Germany), ammonium hydroxide solution (25%) was from Fluka (Switzerland), toluene was from Caledon (Canada), acetone and ethanol were purchased from Fisher scientific (USA). Hydroxyapatite powder (HA) (Type II, particle size of 20 μm) was purchased from Biorad (USA) and used for bone affinity tests. Dialysis tubing (2000 MWCO) was purchased from Spectrum Laboratories (USA).

The following equipment were used in the synthesis and characterization experiments: ultrasonic probe (Sonicator W-375, Heat systems Ultrasonics, USA), homogenizer (Biohomogenizer 1281, Biospec, USA), Atomic Force Microscope (AFM) (BioScope Catalyst, Bruker, USA), Atomic Absorption Spectrometer (Spectra AA 880, Varian, Australia). The FT-IR spectra were recorded on KBr pellets using Nicolet Magna-IR 550 spectrometer (Thermo Scientific, USA). The samples for transmission electron microscopy (TEM) were prepared by placing a drop of suspension on a copper-coated grid and removing excess solution with filter paper and imaging was performed at 80KV using Morgagni (Philips/FEI, USA). Dynamic light scattering (DLS) measurements were performed using Nano-ZS 3600 instrument (Malvern, UK). For X-ray photoelectron spectroscopy (XPS), samples in powder form were submitted for analysis using AXIS Ultra XPS imaging spectrometer (Kratos analytical, Japan). X-ray radiograph of SPIONs targeted to HA powder was captured using Skyscan 1176 in vivo micro-CT (SkyScan, Belgium). All glassware used in synthesis was cleaned with 10% HNO3 prior to use.

2.2. Synthesis of SPIONs. In order to obtain size-controlled nanoparticles with good hydrophilicity, a water-in-oil reversed microemulsion method was employed to synthesis the SPIONs.[13] Briefly, two microemulsions (micro-A and B) with the following compositions were prepared: micro-A was composed of toluene (29 mL) as oil phase and aqueous solution of $FeCl_3$ (202 mg) and $FeCl_2$ (75 mg) at molar ratio of 2:1 in 2.045 mL of deionized (DI) water; micro-B was composed of the same oil phase and 25% ammonium hydroxide solution (2.65 mL) as reducing agent and aqueous phase. In both microemulsions CTAB was used as surfactant with water to surfactant molar ratio kept at 23 by using 1.8 g of CTAB. After preparing the above reagents in different beakers, each was separately mixed by homogenizer at speed of 7000 rpm and 1-butanol was titrated into the above compositions while mixing. Butanol played a role as cosurfactant to help formation of microemulsions, and its addition continued until the color changed from turbid to transparent, indicating formation of stable microemulsions.

After making the microemulsions, micro-A and micro-B were mixed in a three-necked flask using homogenizer (7000 rpm) at 50 °C and under constant flow of N_2 gas. In addition, an ultrasonic probe (5W) was used during the synthesis to prevent the aggregation of nanoparticles. After 60 min, the reaction stopped and the product was cooled down to room temperature, then 20 mL of ethanol was added to the reaction flask to burst the microemulsions. SPIONs were collected with a Neodymium magnet and the supernatant discarded. SPIONs were then washed with boiling ethanol (4×) to remove excess CTAB and further purified by acetone (2×) and DI water (2×). After the washing step with acetone, nanoparticles were well-dispersed and could not be separated with a magnet in a reasonable time (1 day), and hence, they were centrifuged for 10 min (at 5000 rpm) and the pellet was redispersed in 20 mL of DI water using ultrasonic probe at 5W (30 s). The DI water used in all steps was previously deoxygenated by bubbling N_2 through the water for 30 min and passing through Whatman filter paper.

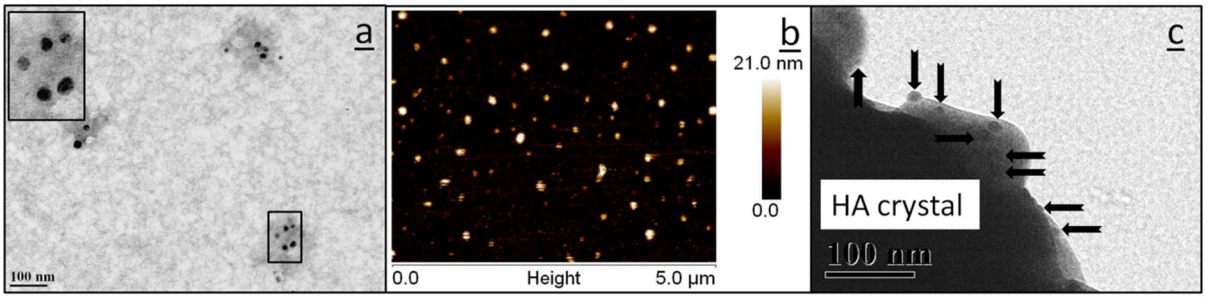

Figure 2. (a) TEM image showing bare SPIONs with spherical shape and average size of 16 nm. (b) Representative AFM image of SPIONs after ALN conjugation showing average size of 17 nm. (c) TEM image representing numerous bone-targeting SPION-ALN targeted to a HA crystal after incubation for 2 h.

Before proceeding, a 50 μL aliquot of final solution was drawn and dissolved in 3 mL of 70% nitric acid and after 2 days submitted for Atomic Absorption Spectrometry (AAS) to measure the iron concentration in the sample. This synthesis method resulted in total Fe content of 40−45 mg in each batch and after all purification steps.

2.3. SPION Functionalization and Alendronate Conjugation. The bare SPIONs were modified with citric acid according to the previously reported procedure[14] to introduce surface carboxylic acid groups for covalent conjugation to amine-terminated BP, ALN. In brief, the synthesized SPIONs were redispersed in DI water at concentration of 2 mg/mL (~72% Fe content) and sonicated for 10 min. The pH of the solution was adjusted to 3.0 by addition of 0.1 M HCl and then citric acid at 5% molar ratio of Fe was added to the suspension (~ 8:1 w/w, e.g., for 2 mg SPIONs, 0.25 mg citric acid was added), in order for anion exchange of OH with COOH and chemisorption. The mixture was stirred for 4h and then washed and purified by magnetic separation (3X). The modified SPIONs were dispersed in sodium phosphate buffer (PB) (pH 7.2, 50 mM) at concentration of 1 mg/mL.

The COOH-modified SPIONs were activated employing EDC/NHS strategy and used for conjugation to ALN. According to the protocol,[15] 2 mg of EDC along with 1.2 mg of NHS (1:1 molar ratio) was dissolved in 0.2 mL PB buffer (pH 7.2, 50 mM) and quickly added to 2 mL (equal to 2 mg of SPIONs) of SPION-COOH suspension and mixed for 30 min at room temperature while using ultrasonic probe (5W). The activated SPIONs were dialyzed (2000 MWCO) against the same buffer for 2h to remove excess EDC and NHS to avoid any unwanted reaction with ALN in the next step (Figure 1).

The activated SPIONs (2 mg) were then redispersed by quick sonication for 30 s and 0.7 mg of predissolved ALN in the same PB buffer was added to the suspension and mixed gently for 3h. Then, the suspension was dialyzed against the same buffer for 24h with 3 changes of buffer. Dialysis of the sample for longer resulted in precipitation of SPIONs and hence was avoided.

2.4. Characterization. The SPIONs conjugated to ALN (SPION-ALN) were characterized by various analytical techniques. TEM and AFM were used to investigate size and morphology of the SPIONs before and after drug conjugation. For TEM measurements, at least 100 nanoparticles from various regions of each grid were manually measured for diameter and averaged. Moreover, DLS was used after each step to record hydrodynamic size as well as zeta potential in 3 different dispersants: DI water, PB (pH 7.2, 50 mM) with zero salt and sodium phosphate buffer saline (PBS) (pH 7.2, 50 mM, 150 mM NaCl). The hydrodynamic sizes were reported based on percent number. The structural characterization in order to confirm conjugation was performed by FT-IR to investigate functional groups and formed bonds, and XPS for surface elemental analysis. Approximately 1 mg of sample was lyophilized for XPS and FT-IR experiments.

2.5. Bone Mineral Affinity Study. To evaluate the affinity of SPION-ALN toward bone, their binding to HA microparticles (average diameter of 20 μm) as the primary mineral of bone were assessed in different dispersants. Typically, 1.5 mL of PB (pH 7.4, 50 mM) containing approximately 50 μg of SPION-ALN or unmodified SPIONs was incubated with 10 mg of HA powder in the dark and gently shaken. After 2h, the supernatant containing unbound nanoparticles was removed by centrifugation at 600 rpm (1 min). The pellet was washed 7 times with 0.2 mL buffer and each time the supernatant was removed and added to the previously collected supernatant. The pellet contained the bound nanoparticles to HA powder. Both components were dissolved in 70% nitric acid and submitted for AAS analysis to measure the Fe concentration. The percent binding calculated as Fe concentration of pellet/(Fe concentration of supernatant + Fe concentration of pellet) × 100. In addition, the binding of nanoparticles to HA powder was measured in presence of different concentrations of NaCl ranging from 50 to 300 mM to prevent nonspecific binding due to ionic interaction. The effect of time on binding of SPION-ALN to HA, evaluated by incubating the sample with HA as explained above, followed by further sampling of the supernatant at 6 and 24 h.

Furthermore, a sample of SPIONs conjugated with Tris instead of ALN and considered as an additional negative control. Tris lacks the phosphonate groups of ALN, but similar to ALN offers one primary amine for conjugation to carboxylic acid groups of modified SPIONs and further has 3 hydroxyl groups at the other end, capable of some binding to HA. The binding of bare SPIONs, SPION-ALN, and SPION-Tris were assessed in presence of various concentrations of rat serum.

3. RESULTS

3.1. SPION Synthesis and Characterization. The size of SPIONs synthesized with the microemulsion technique ranged from 10 to 24 nm with an average of 16 nm (SD = 4.11), when 100 particles were included in the measurement. AFM measurements on SPION-ALN showed the average size of 17 nm that correlated well with TEM results (Figure 2). AFM image (Figure 2b) was recorded in magnetic force microscopy (MFM) mode using a magnetic tip, in other words it only recorded nanoparticles if they were magnetic. The changes in hydrodynamic size and zeta potential of nanoparticles were monitored at each step and in 3 different dispersants using DLS (Figure 3). The size of SPIONs in water and PB were measured 15 and 42 nm, respectively. Although unchanged under TEM, SPIONs after conjugation with ALN experienced an increase in their hydrodynamic size both in water and PB and measured at 61 and 65 nm, respectively. The size of SPIONs coated with COOH (SPION-COOH) and SPIONs activated with EDC/NHS (SPION-Active) both remained the same in water and PB and measured at 15 nm for SPION-COOH and 18 nm in case of SPION-Active. All nanoparticles except SPION-COOH and SPION-Active which slightly increased in their size, experienced some aggregation in PBS and accurate measurement was not accomplished. However, comparison between the polydispersity indexes of SPION-ALN (0.316) and bare SPIONs

dx.doi.org/10.1021/am4010495 | ACS Appl. Mater. Interfaces 2013, 5, 5219−5226

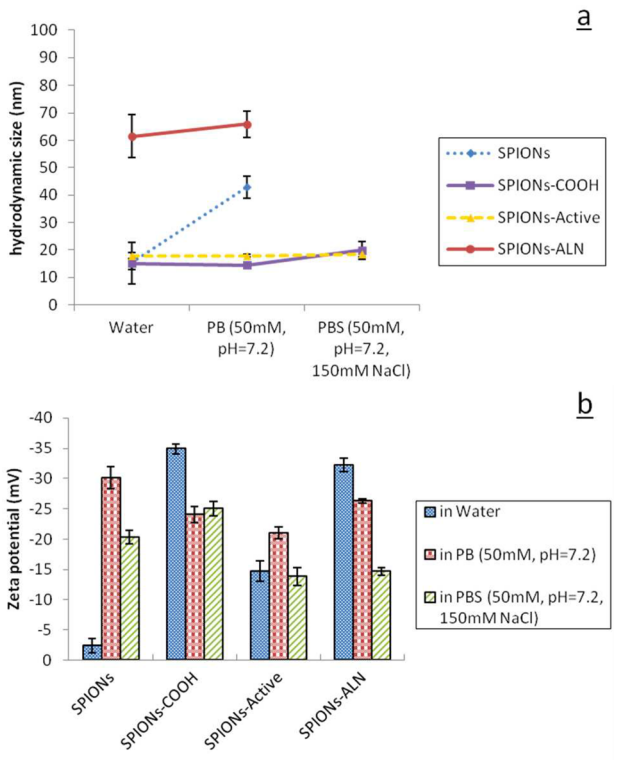

Figure 3. DLS measurements: (a) Graph representing the hydrodynamic size of nanoparticles at each step and in different dispersants. (b) Zeta potentials of suspensions in different dispersants. The error bars are presented as standard deviation.

(0.618) suggests a slight degree of aggregation in the case of SPION-ALN.

The zeta potential of nanoparticles dispersions was recorded in the same dispersant as in the size measurement experiment and served as one of the tools to conclude the formation of citric acid coating, activation and conjugation. The behavior of nanoparticles at each step in water, PB and PBS is presented in Figure 3b. The bare SPIONs in water (pH 7.0) were slightly negatively charged (−2.3 mV) as a result of being slightly above the point of zero charge. After coating the surface of bare SPIONs with citric acid, the surface charge of the nanoparticles changed from −2.3 ± 1.19 mV to −34.9 ± 0.81 mV. Activation of SPION-COOH with EDC/NHS increased the zeta potential to −14.7 ± 1.61 mV. ALN molecule has two phosphonate groups in its structure and as a result, after conjugation to SPION-Active, the surface charge was lowered to −32.2 ± 1.07 mV.

3.2. Alendronate Conjugation. As previously mentioned, ALN as a bisphosphonate has two phosphonate groups in its structure, in other words, each molecule of ALN has two phosphorus atoms. We used this as a means of determining the successful conjugation of ALN to SPIONs. Therefore, a sample of SPION-ALN was synthesized based on the above-mentioned protocol with the only difference of using MES buffer (pH 6.0, 100 mM) instead of PB to provide a synthesis media free of phosphorus, giving us the confidence to relate any phosphorus peak to presence of ALN. After conjugation, the sample was dialyzed against MES buffer for 40 h with 4 changes of buffer, lyophilized and analyzed using XPS. The bare SPION and SPION-COOH showed no phosphorus peak as expected, whereas the SPION-ALN showed the phosphorus peak confirming successful conjugation (Figure 4a−c). The low intensity of phosphorus peak was a result of efforts made to keep the concentration of ALN below therapeutic dose. Also, the absence of strong Fe peaks in SPION-ALN spectra may be attributed to the surface coverage of nanoparticles with ALN molecules.

The FT-IR peak (Figure 5) at 588 cm^{-1} in bare SPIONs spectra revealed that nanoparticles were mostly comprised of Fe_3O_4. The broad peak centered at 3330 cm^{-1} is due to adsorbed molecular water as well as structural OH groups. The peak at 2932 cm^{-1} was assigned to asymmetric CH_2 as a result of remained surfactants and washing solvents and could be removed by repeating the washing steps. Furthermore, FT-IR data was used to confirm the successful conjugation of ALN to SPIONs. ALN has a primary amine group and shows several characteristic bands including NH_2 stretch bands at 3340 and 3489 cm^{-1}, P−OH stretch at 2267 cm^{-1} (broad), NH_2 bending at 1642, and P═O stretch at 1188 cm^{-1}. After amidation reaction, the peaks related to amine disappeared and new peaks associated with amide structure appeared. The peak at 3321 cm^{-1} was assigned to N−H stretch, 2441 cm^{-1} to P−OH, 1716 cm^{-1} to C═O amide, and 1145 cm^{-1} to P═O. The new amide C═O peak and presence of phosphonate peaks in SPION-ALN supported the previously found results of XPS and DLS.

3.3. Bone Affinity Test. SPION-ALN was bound to HA powder at higher percentage in all solutions, compared to bare SPIONs. The highest percentage of binding for both samples was measured in PB at 65% and 37% binding for SPION-ALN and SPIONs, respectively. The percent binding was decreased by incremental addition of salt to the suspensions. This decrease in HA binding was more pronounced in the case of SPIONs, suggesting weak ionic bonds being responsible for the binding. 27% of SPION-ALN stayed bound to HA even at very high salt concentration of 300 mM NaCl compared to 11% for SPIONs. Figure 6 shows the trend of nanoparticles binding to HA in different solutions. The HA binding in complex medium such as rat serum at different concentrations showed to be significantly higher for SPION-ALN compared to bare SPIONs and SPION-Tris. Moreover, the binding of SPION-ALN to HA, confirmed to be strong over time, with 95% of nanoparticles remaining bound after 24 h.

Figure 6d, represents the macroscopic picture of SPION-ALN remaining bound to HA powder after 7 cycles of washing and the associated CT image. The CT image showed approximately 5% increase in the image intensity after incubation of HA powder with SPION-ALN because of thr higher atomic number of iron oxide nanoparticles.

4. DISCUSSION

SPION were synthesized using a microemulsion method in which two microemulsions of water-in-oil were prepared, with solution of iron salts or reducing agent as aqueous phase and toluene as oil phase. Theoretically, each microemulsion consists of nanodroplets that when in reaction, act as nanoreactors and upon mixing of the two, SPIONs will form within the size limit of the nanodroplets.[16] One advantage of this method is to produce water dispersible nanoparticles with relatively narrow size distribution which is very important for bioapplications. As a result, the bare SPIONs dispersed in DI water at concentration of 2 mg/mL remained stable with no obvious sedimentation over the 12 month duration of monitoring. In addition, the ALN-conjugated SPIONs as well as unmodified SPIONs showed good redispersion in DI water and PB after

dx.doi.org/10.1021/am4010495 | ACS Appl. Mater. Interfaces 2013, 5, 5219−5226

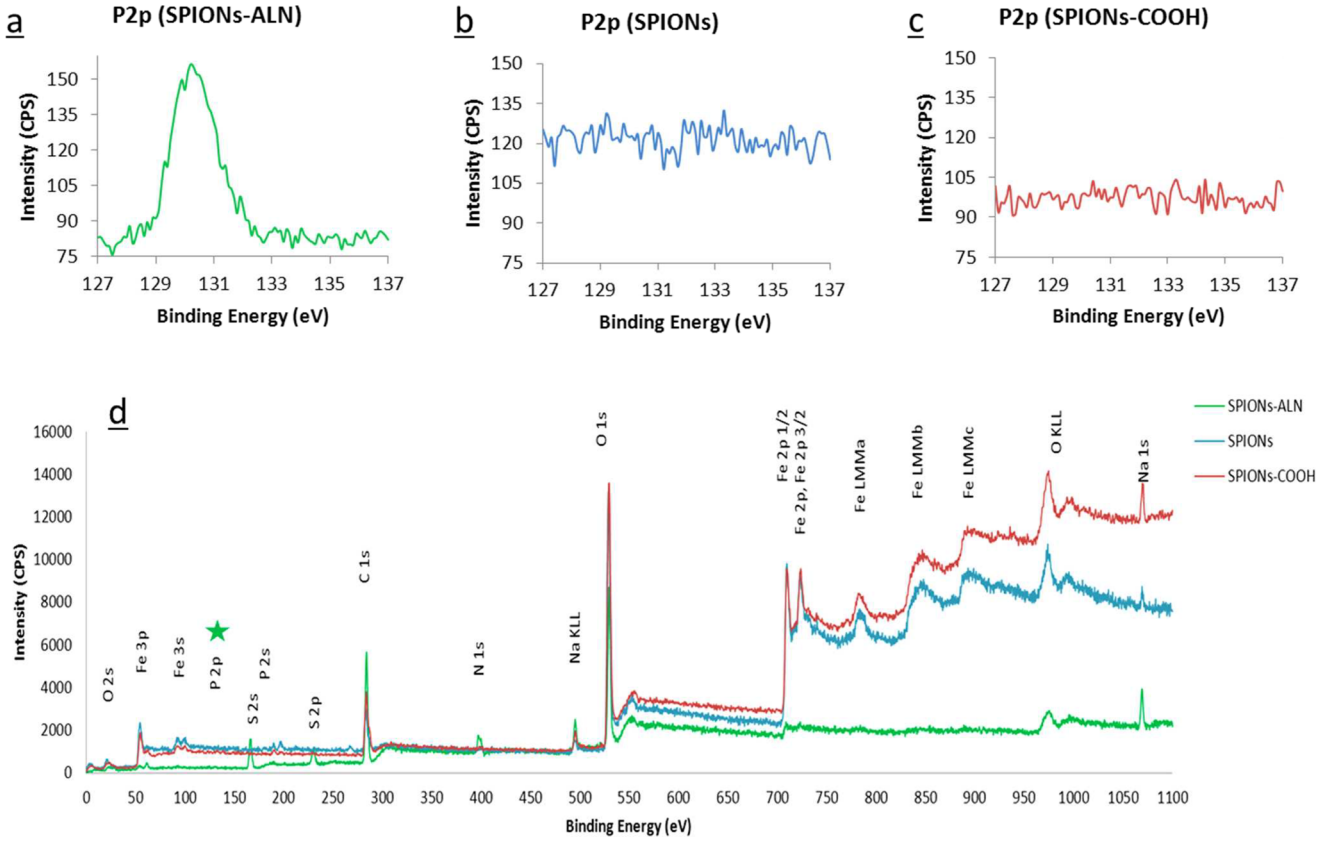

Figure 4. XPS analysis: (a) P2p peak of phosphorus was detected in the SPION-ALN sample and interpreted as an indication of successful conjugation. (b, c) Absence of phosphorus peak in the bare SPION and SPION-COOH samples. (d) Survey spectra showing all elements in the samples.

freeze-drying, without the need for sonication or agitation. The synthesized SPIONs were then modified by addition of citric acid to introduce surface COOH groups. Citric acid via one or two of its carboxylate groups coordinate onto the surface of SPIONs[17] and provides a robust coating, whereas the uncoordinated COOH group(s) contribute to the colloidal stability − partly through charge repulsion while also serving as available sites for further conjugation with ALN. The use of citrate-coated SPIONs with prolonged half-life as MRI angiography contrast agents has been already reported in the literature.[18]

As previously mentioned, the aim of this project was to couple SPIONs covalently to BP drugs employing an amide linkage for future use in MRI imaging of bone metabolic activity. The SPION-COOH would naturally react with amine group of ALN; however, that reaction would be very slow and of low yield. Therefore, after COOH modification, EDC/NHS as a zero-length cross-linker was selected to conjugate SPIONs with the NH_2-terminated BP (e.g., ALN). This is a very common strategy in bioconjugation and has been employed extensively to conjugate antibodies[19,20] and other NH_2-terminated compounds and materials to SPIONs.[21] EDC is water-soluble and forms active ester for coupling with amines. However, the higher yield in the reaction is achievable by addition of NHS or the more water-soluble form of that, sulfo-NHS, to form NHS ester. By intermediation of EDC/NHS, the reactivity of the molecules was significantly enhanced. Another advantage of the EDC/NHS method is to covalently bind SPIONs to BP through an amide linkage in a quick reaction without leaving any fragment of EDC or NHS molecules in the final product. The formation of all reactants was monitored by FT-IR, DLS, and XPS step by step. The appearance of P 2p peak on XPS after conjugation with ALN served as an indication of successful production of the bone-seeking probe as there was no phosphorus in the reagents that were used in previous steps. Moreover, amide peak in the SPION-ALN sample as well as appearance of P═O and P−OH associated peaks on FT-IR correlated well with the previously found results. Conversion of zeta potential form −15 mV in NHS-activated SPIONs to −32 mV after conjugation with ALN due to phosphonate groups of ALN served as another indicator, since ALN in physiological pH is completely ionized and possesses negative charge. The most important evidence and confirmation was achieved by observing the enhancement in binding of SPION-ALN to HA powder. Although the lack of a previous report makes it is difficult to assess whether or not the in vitro binding of 65% to HA suffices for imaging purposes, the ability to tune the number of ALNs attached to SPIONs' surface, which directly controls the binding to bone, offers the capability of increasing the binding even further in case it is required.

It is now well-recognized that the surface of nanoparticles would be covered by proteins upon their entrance to the biological medium.[22] This protein coverage is controlled by various pathways in human body.[23] Recent results both from our group[24,25] and others,[26] have shown the critical importance of the suspending medium on targeting capability of nanoparticles. To clarify this matter, we have performed the HA binding test in the presence of rat serum. Similar to PB buffer, the SPION-ALN revealed higher binding to HA compared to

dx.doi.org/10.1021/am4010495 | ACS Appl. Mater. Interfaces 2013, 5, 5219−5226

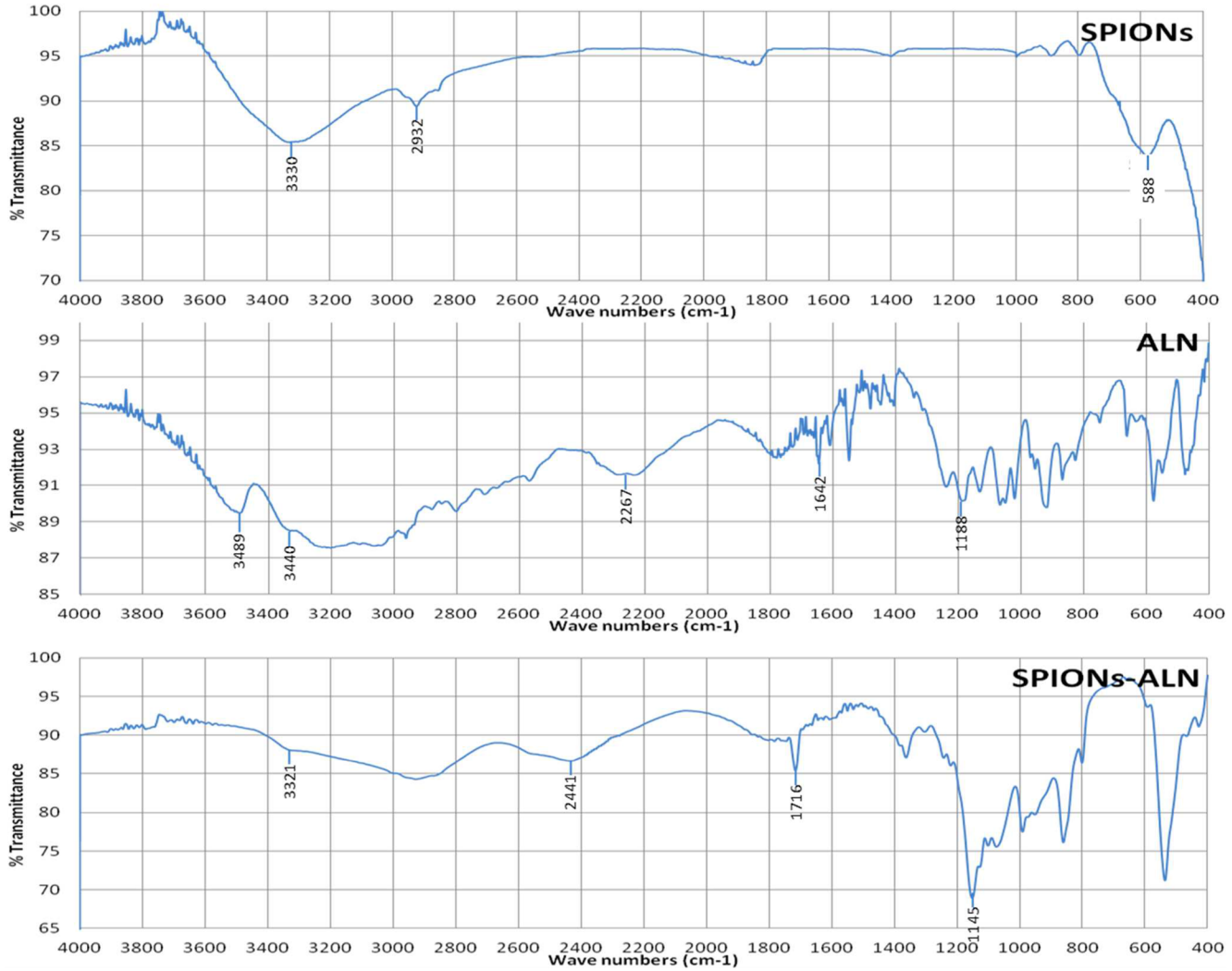

Figure 5. FT-IR spectra: Note the presence of amide peak at 1716 cm^{-1}in SPION-ALN as well as phosphonate peaks at 1145 cm^{-1} (P═O) and 2441 cm^{-1} (P−OH).

bare SPIONs (Figure 6b). Furthermore, the equal or close binding to HA does not necessarily mean that bare SPIONs will have the same in vivo behavior. In fact, it has already shown that bare SPIONs do not target bone.[27] After IV injection, opsonin proteins (such as fibrinogen) will cover the surface of bare SPIONs immediately and consequently macrophages remove them from bloodstream. On the other hand, we are optimistic that our novel tracer will manifest 'stealth properties' due to its citric acid coating, and target bone because of its BP moiety. However, the actual required dose of the SPION-ALN to produce reasonable contrast on MRI requires further in vivo experimentation and validation. Pharmacokinetics studies show that approximately 60% of ALN can be uptaken by skeleton after intravenous injection.[28]

Iron oxide nanoparticles coated (anchored) with BPs have been used in bioapplications previously, for instance, in labeling of stem cells to investigate their differentiation and migration.[29] Motte and co-workers have conducted a significant amount of research on those types of nanoparticles. However, they have mostly focused on the reported anticancer properties of BPs.[30,31] In one report,[32] they exploited the chelating properties of BP to anchor them on the surface of SPIONs and proposed future potential use in imaging; however, the dose of BP used in synthesis was very high. Also, Sandiford et al.[9] have employed a similar approach and reported the production of long circulating ^{99m}Tc-labeled SPIONs as a dual modality MRI-SPECT contrast agent for cardiovascular system imaging. Although that strategy has proven to be effective for the sake of anticancer research or imaging of the cardiovascular system, it neutralizes bone seeking activity by using the phosphonate "arms" to impart attachment to SPIONs. Therefore, for dynamic imaging of metabolic bone activity, it is essential to preserve the phosphonate moieties to impart subsequent bone mineral affinity.

5. CONCLUSION

In this work, a relatively simple and cost-effective method was employed to conjugate ALN covalently to SPIONs (patent pending) for future use as a nonionizing dynamic contrast agent in MRI imaging of bone. To best of our knowledge, this is the first report of bone-targeting iron oxide nanoparticles for potential use with the imaging of bone turnover. The conjugative strategies presented here may serve as a novel platform of nonionizing dynamic bone imaging tracers, capable of detecting bony adaptation prior to their radiological manifestation.

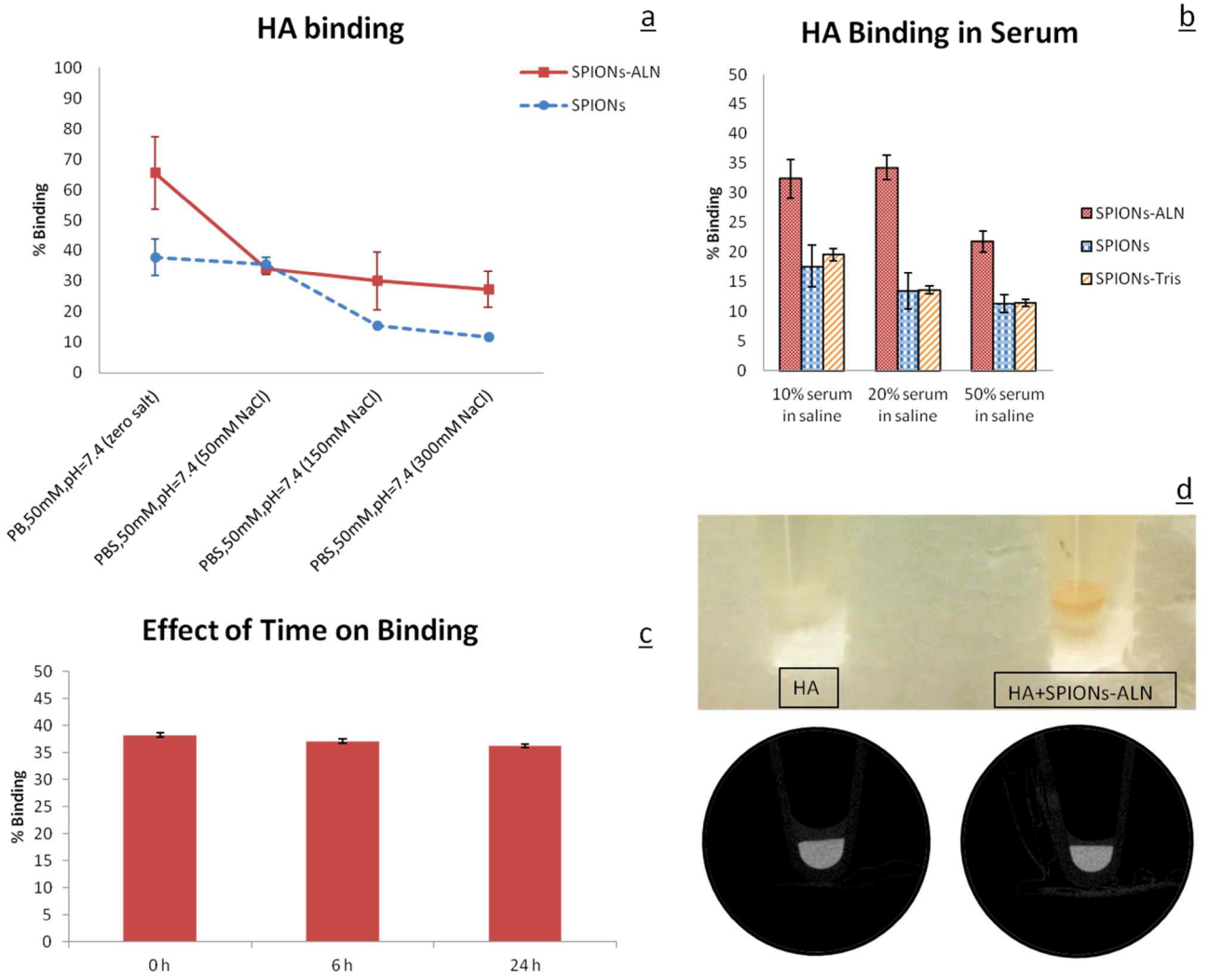

Figure 6. HA binding: (a) Note that SPION-ALN was less susceptible to loss of binding by increasing the concentration of NaCl from 50 mM to 300 mM. (b) HA binding in rat serum showing significantly higher binding for SPION-ALN in all concentrations. (c) Graph represents negligible loss (<5%) of binding to HA over time for SPION-ALN. (d) Macroscopic image of HA powder (left) and HA powder incubated with SPION-ALN in PB (50 mM, pH 7.4) after washing process and their corresponding CT cross-sectional slices. The error bars present standard deviation.

AUTHOR INFORMATION

Corresponding Author

*E-mail: mdoschak@ualberta.ca.

Author Contributions

The manuscript was written through contributions of all authors. All authors have given approval to the final version of the manuscript.

Notes

The authors declare no competing financial interest.

ACKNOWLEDGMENTS

This research was funded by the Osteoarthritis Alberta Team Grant from Alberta Innovates – Health Solution (AIHS).

ABBREVIATIONS

SPIONs, superparamagnetic iron oxide nanoparticles
MRI, magnetic resonance imaging
OA, Osteoarthritis
BP, bisphosphonates
ALN, alendronate
CTAB, hexadecyltrimethylammonium bromide
EDC, N-ethyl-N′-[3(dimethylamino)propyl]carbodiimide hydrochloride
NHS, N-hydroxysuccinimide
TEM, transmission electron microscopy
DLS, dynamic light scattering
XPS, X-ray photoelectron spectroscopy
AAS, atomic absorption spectrometry
FT-IR, Fourier transform infrared spectroscopy

REFERENCES

(1) Lawrence, R. C.; Felson, D. T.; Helmick, C. G.; Arnold, L. M.; Choi, H.; Deyo, R. A.; Gabriel, S.; Hirsch, R.; Hochberg, M. C.; Hunder, G. G.; Jordan, J. M.; Katz, J. N.; Kremers, H. M.; Wolfe, F. *Arthritis Rheum.* **2008**, *58*, 26−35.

(2) Kim, H. R.; So, Y.; Moon, S. G.; Lee, I. S.; Lee, S. H. *Osteoarthr. Cartil.* **2008**, *16*, 212−218.

(3) McCrae, F.; Shouls, J.; Dieppe, P.; Watt, I. *Ann. Rheum. Dis.* **1992**, *51*, 938−942.

(4) Burr, D. B. *J. Rheumatol.* **2005**, *32*, 1156−8.

(5) Dieppe, P.; Cushnaghan, J.; Young, P.; Kirwan, J. *Ann. Rheum. Dis.* **1993**, *52*, 557−563.

(6) Panahifar, A.; Maksymowych, W. P.; Doschak, M. R. *Osteoarthr. Cartil.* **2012**, *20*, 694−702.

(7) Mahmoudi, M.; Hosseinkhani, H.; Hosseinkhani, M.; Boutry, S.; Simchi, A.; Journeay, W. S.; Subramani, K.; Laurent, S. *Chem. Rev.* **2011**, *111*, 253−280.
(8) Mahmoudi, M.; Hofmann, H.; Rothen-Rutishauser, B.; Petri-Fink, A. *Chem. Rev.* **2012**, *112*, 2323−2338.
(9) Sandiford, L.; Phinikaridou, A.; Protti, A.; Meszaros, L. K.; Cui, X.; Yan, Y.; Frodsham, G.; Williamson, P. A.; Gaddum, N.; Botnar, R. M.; Blower, P. J.; Green, M. A.; de Rosales, R. T. *ACS Nano* **2013**, *7*, 500−512.
(10) Lalatonne, Y.; Paris, C.; Serfaty, J. M.; Weinmann, P.; Lecouvey, M.; Motte, L. *Chem. Commun. (Camb)* **2008**, *22*, 2553−5.
(11) Russell, R. G.; Watts, N. B.; Ebetino, F. H.; Rogers, M. J. *Osteoporos. Int.* **2008**, *19*, 733−759.
(12) Barja, B. C.; Herszage, J.; dos Santos Afonso, M. *Polyhedron* **2001**, *20*, 1821−1830.
(13) Maleki, H.; Simchi, A.; Imani, M.; Costa, B. F. O. *J. Magn. Magn. Mater.* **2012**, *324*, 3997−4005.
(14) Fan, H. M.; Olivo, M.; Shuter, B.; Yi, J. B.; Bhuvaneswari, R.; Tan, H. R.; Xing, G. C.; Ng, C. T.; Liu, L.; Lucky, S. S.; Bay, B. H.; Ding, J. *J. Am. Chem. Soc.* **2010**, *132*, 14803−14811.
(15) Hermanson, G. *Bioconjugate Techniques*, 2nd ed.; Academic Press: New York, 2008; pp 595−599.
(16) Lawrence, M. J.; Rees, G. D. *Adv. Drug Delivery Rev.* **2000**, *45*, 89−121.
(17) Kallay, N.; Matijevic, E. *Langmuir* **1985**, *1*, 195−201.
(18) Wagner, S.; Schnorr, J.; Pilgrimm, H.; Hamm, B.; Taupitz, M. *Invest. Radiol.* **2002**, *37*, 167−177.
(19) Hadjipanayis, C. G.; Machaidze, R.; Kaluzova, M.; Wang, L.; Schuette, A. J.; Chen, H.; Wu, X.; Mao, H. *Cancer Res.* **2010**, *70*, 6303−6312.
(20) Dilnawaz, F.; Singh, A.; Mohanty, C.; Sahoo, S. K. *Biomaterials* **2010**, *31*, 3694−3706.
(21) Wang, C.; Irudayaraj, J. *Small* **2010**, *6*, 283−289.
(22) Mahmoudi, M.; Lynch, I.; Ejtehadi, M. R.; Monopoli, M. P.; Bombelli, F. B.; Laurent, S. *Chem. Rev.* **2011**, *111*, 5610−5637.
(23) Ghavami, M.; Saffar, S.; Abd Emamy, B.; Peirovi, A.; Shokrgozar, M. A.; Serpooshan, V. *RSC Adv.* **2013**, *3*, 1119−1126.
(24) Mirshafiee, V.; Mahmoudi, M.; Lou, K.; Cheng, J.; Kraft, M. L. *Chem. Commun. (Camb)* **2013**, *49*, 2557−2559.
(25) Laurent, S.; Mahmoudi, M. *Int. J. Mol. Epidemiol. Genet.* **2011**, *2*, 367−390.
(26) Salvati, A.; Pitek, A. S.; Monopoli, M. P.; Prapainop, K.; Bombelli, F. B.; Hristov, D. R.; Kelly, P. M.; Aberg, C.; Mahon, E.; Dawson, K. A. *Nat. Nanotechnol* **2013**, *8*, 137−143.
(27) Jalilian, A. R.; Panahifar, A.; Mahmoudi, M.; Akhlaghi, M.; Simchi, A. *Radiochim. Acta* **2009**, *97*, 51−56.
(28) Lin, J. H.; Duggan, D. E.; Chen, I. W.; Ellsworth, R. L. *Drug Metab. Dispos.* **1991**, *19*, 926−932.
(29) Delcroix, G. J.; Jacquart, M.; Lemaire, L.; Sindji, L.; Franconi, F.; Le Jeune, J. J.; Montero-Menei, C. N. *Brain Res.* **2009**, *1255*, 18−31.
(30) Benyettou, F.; Lalatonne, Y.; Sainte-Catherine, O.; Monteil, M.; Motte, L. *Int. J. Pharm.* **2009**, *379*, 324−327.
(31) Benyettou, F.; Lalatonne, Y.; Chebbi, I.; Di Benedetto, M.; Serfaty, J. M.; Lecouvey, M.; Motte, L. *Phys. Chem. Chem. Phys.* **2011**, *13*, 10020−10027.
(32) Lalatonne, Y.; Monteil, M.; Jouni, H.; Serfaty, J. M.; Sainte-Catherine, O.; Lievre, N.; Kusmia, S.; Weinmann, P.; Lecouvey, M.; Motte, L. *J. Osteoporos.* **2010**, *2010*, 747852.